Sains Malaysiana 51(9)(2022): 2937-2954
http://doi.org/10.17576/jsm-2022-5109-16

Zirconium(IV)-BTC-Based MOF Modified with Nickel as a Catalyst for Hydrogenation of Citronellal

(Zirkonium(IV)-BTC-Berdasarkan MOF Terubah Suai dengan Nikel sebagai Pemangkin untuk Penghidrogenan Sitronela)

WITRI WAHYU LESTARI[1,*], ARIFTI NUR LAILY AQNA[1], FAUZAN IBNU PRIHADIYONO[1], RIANDY PUTRA[1], MAULIDAN FIRDAUS[1], VENANSIA AVELIA ROSARI[1], UBED SONAI FAHRUDIN ARROZI[2] & GRANDPRIX T. M. KADJA[3,4,5]

[1]*Department of Chemistry, Faculty of Mathematics and Natural Sciences, Sebelas Maret University, Jl. Ir Sutami No. 36A, Kentingan-Jebres, Surakarta, Central Java, Indonesia*
[2]*Department of Chemistry, Faculty of Mathematics and Science, State University of Malang, Jl. Semarang 5, Malang 65145, East Java, Indonesia*
[3]*Division of Inorganic and Physical Chemistry, Faculty of Mathematics and Natural Sciences, Institut Teknologi Bandung, Jl. Ganesha No. 10, Bandung 40132, Indonesia*
[4]*Center for Catalysis and Reaction Engineering, Institut Teknologi Bandung, Jl. Ganesha No. 10, Bandung 40132, Indonesia*
[5]*Research Center for Nano sciences and Nanotechnology, Institut Teknologi Bandung, Jl. Ganesha No. 10, Bandung 40132, Indonesia*

Received: 14 January 2022/Accepted: 19 April 2022

ABSTRACT

This study is designed to determine the effect of nickel (Ni) metal bearing on zirconium(IV) benzene 1,3,5-tricarboxylate based MOF, $[Zr_6O_4(OH)_4(O_2C_2H_3)_6(BTC)_2]$ (Zr-BTC) and its application as a catalyst in the citronellal hydrogenation. The synthesis of Zr-BTC was carried out under solvothermal condition, while the wet impregnation method was used to synthesize 2.5 wt.% Ni/Zr-BTC. The catalytic test of citronellal hydrogenation was performed in a batch reactor at 80 °C for 6 h with various hydrogen pressures. XRD characterization showed the suitability of the prominent peaks of Zr-BTC to the standard pattern, while Ni metal could not be detected clearly but was confirmed by EDX analysis. FTIR analysis showed a significant shift in the wavenumber from 1722 cm^{-1} to 1567 cm^{-1} indicating coordination of deprotonated ligands to the Zr^{4+} metal ions. Nickel loading reduced the surface area of Zr-BTC to 523 m^2/g and the pore volume to 0.11 cc/g according to the nitrogen sorption isotherm. The catalytic tests showed that 30% Ni loading enhanced the activity and selectivity of Zr-BTC in citronellal hydrogenation, resulting in 62.1% yield of isopulegol (for batch reactor) and 14.1% yield of citronellol (for hydrogen balloon).

Keywords: Catalyst; citronellal; hydrogenation; MOFs; Ni/Zr-BTC

ABSTRAK

Kajian ini adalah untuk menentukan kesan galas logam nikel (Ni) ke atas zirkonium(IV) benzena 1,3,5-trikarboksilat berasaskan MOF, $[Zr_6O_4(OH)_4(O_2C_2H_3)_6(BTC)_2]$ (Zr-BTC) dan penggunaannya sebagai pemangkin dalam penghidrogenan sitronela. Sintesis Zr-BTC telah dijalankan dalam keadaan solvoterma, manakala kaedah impregnasi basah digunakan untuk mensintesis 2.5 wt.% Ni/Zr-BTC. Ujian pemangkin hidrogenasi sitronelal dilakukan dalam reaktor kelompok pada suhu 80 °C selama 6 jam dengan pelbagai tekanan hidrogen. Pencirian XRD menunjukkan puncak tajam pada Zr-BTC sepadan dengan puncak piawai, manakala logam Ni tidak dapat dikesan dengan jelas tetapi disahkan oleh analisis EDX. Analisis FTIR menunjukkan perubahan ketara pada nombor gelombang daripada 1722 cm^{-1} kepada 1567 cm^{-1} yang menunjukkan koordinasi ligan terdeprotonasi kepada ion logam Zr^{4+}. Pertambahan nikel telah mengurangkan luas permukaan Zr-BTC kepada 523 m^2/g dan isi padu liang kepada 0.11 cc/g mengikut isoterma penyerapan nitrogen. Ujian pemangkin pula mendedahkan bahawa penambahan 30% Ni meningkatkan aktiviti dan kepemilihan Zr-BTC dalam penghidrogenan sitronelal, seterusnya menghasilkan 62.1% isopulegol (untuk reaktor kelompok) dan 14.1% sitronelo (untuk belon hidrogen).

Kata kunci: MOFs; Ni/Zr-BTC; pemangkin; penghidrogenan; sitronelal

Introduction

Essential oils obtained from lemongrass (*Cymbopogon nardus*) are commonly used as raw materials for perfume production. It has three main components, i.e., citronellal 32-45%; geraniol 12-18%; and citronellol 12-15% (Guenther 1982). As citronellol has more health benefits and ready to use for antiseptic and antibacterial application (Qneibi et al. 2019), an effort to increase the economic value of the other components are needed, particularly for citronellal as the dominant component. For instance, reduction of citronellal to form citronellol and its derivatives can be carried out by using sodium borohydride ($NaBH_4$) or lithium aluminum hydride ($LiAlH_4$) as a reducing agent (O'Brien & Wicht 2008). However, both reduction agents are dangerous and not environmentally friendly. Based on the principle of green chemistry, heterogeneous catalysts offer several advantages, including easy separation, high thermal stability, preventing corrosion, and reusability (Horcajada et al. 2007; Park et al. 2010). For example, hydrogenation reaction of citronellal with a Ru/SiO_2 catalyst resulted citronellol with selectivity up to 78.2% (Milone et al. 1999). Ni/Zr-beta catalyst was also reported to give 96% of citronellal conversion with 8% citronellal selectivity (Nie et al. 2007). Pt/MWCNTs catalyst has been shown to have 22.6% selectivity to citronellol from 66.5% citral conversion (Qu et al. 2015), while citronellal hydrogenation with $RuSiO_2$ yielded 50% isopulegol (Milone et al. 1999).

Among various porous materials, Metal-Organic Frameworks (MOFs) are one of the promising materials used for heterogeneous catalysts in various organic transformations. MOFs are porous materials composed of metal ions or metal-oxide clusters as nodes and organic ligands as linkers. Due to their structural and functional capabilities, MOFs have become materials of interest to scientists (Yuan et al. 2018). In catalytic application, MOFs have a high surface area and pore size that facilitate diffusion and interface contact between the active site and the reagents (Hanif et al. 2018). In addition, the flexibility in designing MOF facilitates the modification of its catalytic sites. The inorganic components in the MOF structure can function as active sites through the coordinated unsaturated metal ions or their redox properties (Lestari et al. 2021). Moreover, organic ligands bearing certain functional groups can also act as coordination points of active metal species. MOFs' pore can also be efficiently used to encapsulate metal or metal oxide nanoparticles, which could bring a new catalytic function (Cirujano et al. 2012).

Several MOFs have been used as hydrogenation catalysts, including Pd@MIL-101 for the synthesis of (−)-menthol from citronellal (Cirujano et al. 2012), Ni@MOF-5 for crotonaldehyde hydrogenation (Zhao et al. 2012), Ru/Zr-MOF for furfural hydrogenation to furfuryl alcohol (Yuan et al. 2015) and ZJU-28 and MIL-101 (Rh)-SO_3 for 1-octene and 2,3-dimethylbutene hydrogenation (Genna et al. 2016). MOFs are continuing to be developed, and several innovations have been made in the past decade, including metals insertion to produce catalysts with a better catalytic performance.

Nickel is abundant in nature, low cost, and has high activity and selectivity for catalytic hydrogenation reactions, making it considerably intriguing. For example, 3 wt.% Ni/MCM-41 was reported to be highly active in hydrogenation reaction of CO_2 to methane (Zhao et al. 2018). Ni has also been widely used as an active site in MOFs structure, such as Ni/MOF-5 for crotonaldehyde hydrogenation (Plessers et al. 2016), Ni/MesMOF-1 for nitrobenzene hydrogenation or hydrogenolysis of styrene (Park et al. 2010), Ni/UiO-66 for CO_2 methanation (Zhao et al. 2018), Ni/MIL-101 catalyst for CO_2 methanation (Zhen et al. 2017) and Ni-promoted MOF supported on MCM-41 composites for highly-efficient *p*-nitrophenol hydrogenation (Zong et al. 2021).

Zr(IV) based MOF was first synthesized in 2008 and attracted considerable interest due to its chemical and physical stability. These features are necessary for its development as a catalyst and catalyst support (Yuan et al. 2015). In addition, Zr(IV)-based MOFs are non-toxic and environmentally friendly (Zhao et al. 2018). The combination of hard acid-base from Zr(IV) and carboxylate organic linkers significantly increases the strength of the coordination bond, making Zr-MOFs as one of the most stable MOF constructions (Bai et al. 2016; Kim & Cohen 2012). The structure of zirconium-based MOFs is increasingly developed by changing organic linkers, including amino-terephthalate (Kandiah et al. 2010), metalloporphyrin (Feng et al. 2012), porphyrin or cruciform (Morris et al. 2012) and 1,3,5-benzenetricarboxylate (BTC) (Liang et al. 2014). Similarly, various synthetic methods have been developed, such as microwave irradiation (Ren et al. 2014), electrochemical deposition (Stassen et al. 2015), reflux (Cirujano et al. 2015) and solvent-free mechanochemistry (Reinsch et al. 2015; Užarević et al. 2016). Among the reported Zr-based MOFs is Zr-BTC which is composed by Zr(IV) ions coordinated to BTC^{3-} ligands (Liang et al. 2014). This MOF has been reported as hydrogen storage material by immobilizing

Pd nanoparticle in its structure (Xu et al. 2019). Zr-BTC has also been reported as a catalyst for various organic transformations (Hwang et al. 2017).

Considering the importance of nickel as active species in hydrogenation of citronellal and the versatility of Zr-BTC, this work was focused on developing highly stable and porous Zr-BTC as catalyst in hydrogenation of citronellal by passivating nickel as the active species in the catalytic reaction. The employment of Ni is expected to increase the number of exposed active sites, resulting in optimal catalytic activity and selectivity.

Materials and Methods

Materials

The materials used were analytical grade without further purification. Zirconium tetrachloride (98%), acetic acid (100%), dimethylformamide (98%), methanol (99.9%), ethanol (99.9%), and toluene (99.9%) were commercially provided by Merck EMSURE. Benzene 1,3,5-tricarboxylic acid (H_3BTC, 95%), nickel acetylacetone (99%), citronellal oil (≥ 95%), and 2-propanol (99.5%) were purchased from Sigma Aldrich, Germany. Commercial citronellal oil (≥ 95%) used in the catalytic test was further purified by distilling under vacuum. Technical acetone was commercially supplied by Brataco Chemika. Nitrogen gas (UHP 99%) and hydrogen gas (UHP 99%) were purchased from Samator, Indonesia.

Synthesis of Zr-BTC

The synthesis of Zr-BTC was carried out using the solvothermal method. A total of 0.1165 g (0.50 mmol) of $ZrCl_4$ was mixed with 0.0353 g (0.168 mmol) of H_3BTC, 2.8 mL of CH_3COOH as modulator, and 5 mL of DMF in a Teflon line stainless steel. The solution was stirred for 15 min followed by sonication for 20 min. The reaction solution was heated at 135 °C for 24 h and allowed to cool to room temperature. The obtained white precipitate was washed with DMF (2 × 30 mL), methanol (2 × 30 mL), and acetone (2 × 30 mL), then dried at room temperature, and activated using the solvent exchange method with chloroform (30 mL, for 5 days), followed by evaporation at room temperature.

Preparation of Nickel Modified Zr-BTC

Nickel modified Zr-BTC was made using wet impregnation and stirring at room temperature. A total of 1.0 g of $Ni(acac)_2$ was dissolved in 150.0 mL ethanol to yield a dark green solution at 60 °C. A total of 2.0 g Zr-BTC was added to the solution with continuous stirring for 2 h. The solution was filtered and vacuum dried at 60 °C for 2 h to produce a green powder $Ni(acac)_2$/Zr-BTC. The $Ni(acac)_2$/Zr-BTC was reduced under the hydrogen flow (15 mL/min) at 150 °C for 3 h. After the reduction process, a dark yellow solid was obtained as Ni/Zr-BTC. The nickel loading was observed to be 2.5 wt.%.

Catalytic Study of Ni/Zr-BTC Using a Batch Reactor

The citronellal hydrogenation reaction was performed using 0.5 mL citronellal, 50 mL 2-propanol as the solvent. The catalyst concentration used was varied, i.e., 10, 20, and 30 wt.% of Ni contained in Zr-BTC (weight percent of Ni contained in Zr-BTC was calculated in accordance of citronellal mass used in the catalytic reaction). The reaction mixture was added to a 100 cm^3 autoclave reactor. The autoclave was connected to a condenser and a distillate tube to drain steam and other gas produced during the catalytic test process. The catalytic reaction was conducted with 10 bar of H_2 at a stirring speed of 550 rpm for 6 h at 80 °C (Putra et al. 2018). After the reaction, the resulting mixture was filtered to separate the catalyst from the solution.

Catalytic Study of Ni/Zr-BTC Using a Hydrogen Balloon

In a three-neck flask, 0.5 mL citronellal and 10 mL 2-propanol solvent were added and then flowed with nitrogen gas. Subsequently, the catalyst was added to the three-neck flask. The three-neck flask was connected to the condenser and to a balloon filled with H_2 gas (1 bar) and a vacuum pump line. The hydrogenation reaction was performed for 6 h at 80 °C. After the reaction, the resulting mixture was filtered to separate the catalyst from the solution.

Materials Characterization

To analyse the functional groups, a Shimadzu IR Prestige-21 Fourier transforms infrared (FTIR) was used. The materials crystallinity and purity were analysed by X-ray diffraction (XRD) with Cu-Kα (λ = 0.15405 nm) radiation (40 kV) (Rigaku Miniflex 600 Benchtop). Thermo gravimetry/differential thermal analysis (TG-DTA) (Hitachi STA 7000) was conducted to measure the thermal stability of materials. Elemental composition and material morphology were investigated by scanning electron microscopy-energy dispersion

X-ray (SEM-EDX) (Hitachi SU-3500). Transmission electron microscopy (TEM) (Hitachi HT7700) was utilized to determine the distribution of nickel metal in the material. The porosity and surface area of the material were observed using surface area analyser (SAA) (Quadradsorb Evo N_2) analysis. Gas chromatography-mass spectrometry (GC-MS) (Shimadzu QP 2010S) was used to determine the mass spectra and fragmentation of the hydrogenation reaction products. In addition, the selectivity was defined using Equations (1), according to Lestari et al. (2021):

$$S = \frac{Y}{C} x\ 100\% \quad (1)$$

where Y is the yield of citronellol or isopulegol or specific product, as determined by GC analysis, and C is the conversion of citronellal (%).

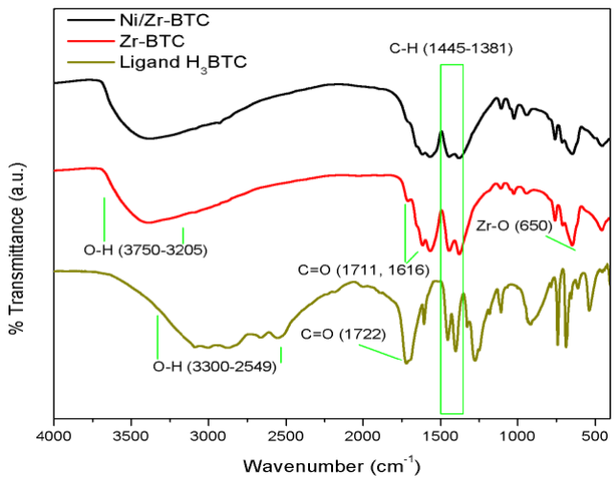

FIGURE 1. FTIR spectra of H_3BTC, synthesized Zr-BTC, and Ni/Zr-BTC

Results and Discussion

Materials Characterization

The successful coordination of H_3BTC ligands to the Zr(IV) ions to form Zr-BTC was indicated by the shifting in the absorption peak from several functional groups compared to free H_3BTC ligands, as shown in Figure 1.

The stretching vibration of the C=O of the carboxylic group from free H_3BTC at 1722 cm^{-1} shifted to 1711 cm^{-1}, indicating the deprotonation of the carboxylate group and the formation of coordination bonds to Zr(IV) ions. The absorption band appears at 650 cm^{-1} indicates the formation of a Zr–O bond (Cavka et al. 2008). Moreover, a new absorption band also appeared at wavenumber 1616 cm^{-1} corresponding to the coordinated acetate group originating from the modulator (Liang et al. 2014). Aside of the carbonyl group, the hydroxyl group (O−H) also exhibited a dramatic alteration within the FITR spectra (Figure 1). In free H_3BTC, the O–H vibration, originating from the carboxylic acid group, appeared as a broad band located at around 3300-2549 cm^{-1}. After forming the Zr-BTC, this band underwent a blue shift to around 3750-3205 cm^{-1} because of the water molecules trapped within the inner structure of Zr-BTC (Larasati et al. 2017). The aromatic C–H absorption band at 3100-3050 cm^{-1} and aliphatic C–H at 3000-2850 cm^{-1} originated from the benzene group with a weak intensity. Figure 1 also shows the FTIR spectra of Zr-BTC impregnated with Ni. After Ni modification, the FTIR spectra did not undergo a significant change, showing that the presence of Ni within the Zr-BTC structure did not alter the local structure of Zr-BTC to a notable extent.

The X-ray diffractogram of Zr-BTC compared to the standard pattern (CCDC No. 1002672) is shown in Figure 2. There is an agreement between the main peaks of the Zr-BTC material with the standard pattern at 2θ = 8.3° (3 1 1), 8.6° (2 2 2), 10.1° (3 3 1), and 10.9° (4 0 0). This peaks indicates the formation of Zr-BTC (Liang

et al. 2014). The high intensity of the diffractogram peaks shown in Figure 2 confirms the high purity of the material. This result was further quantitatively analysed by refinement using the Le Bail method by inserting various cell parameters from the possible phases of the samples derived from CCDC and JCPDS (ESI Figure S1 & Table S1). In the refinement of the synthesized Zr-BTC material, two phases were used: Zr-BTC and H_3BTC (Table S2) (Furukawa et al. 2014). The refinement results showed %R_p of 7.09 and %R_{wp} of 4.79, and GoF of 0.231. This result showed that the structure of the synthesized Zr-BTC was qualitatively consistent with that of the standard.

Ni loading was observed to slightly reduce the Zr-BTC degree of crystallinity to 90.5%. In this study, the presence of Ni could not be detected by XRD since no clear peak of Ni was observed in the diffractogram (Figure 3). In refining the Ni/Zr-BTC, the phase used was the Ni and Zr-BTC standard. The refinement result of Ni/

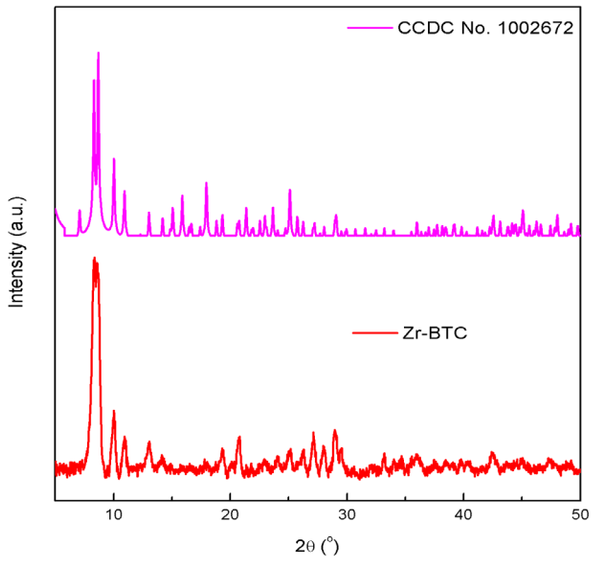

FIGURE 2. Diffractogram of Zr-BTC synthesized and CCCD standard No. 1002672

Zr-BTC showed 8.24 for %R_p, 8.64 for %R_{wp}, and 0.462 for GoF (ESI Figure S2 & Table S1). These low values indicate that Ni/Zr-BTC possessed a similar phase as the existing phases (Ni and Zr-BTC phases). Thus, SEM-EDX would facilitate detecting the presence of Ni as well as its distribution throughout crystals.

The effect of Ni loading on Zr-BTC morphology was analysed using SEM. Figure 4(a) and Figure 4(b) shows the SEM images of Zr-BTC and Ni/Zr-BTC, respectively. We observed that Zr-BTC had an irregular morphology (Li et al. 2018). The impregnation of Ni into Zr-BTC might lead to the coverage of Zr-BTC with Ni metal particles. Ni was dispersed not only on the surface but also in the interior of Zr-BTC, as shown by the TEM images (Figure 4(d)). Based on Figure 4(a) and 4(b), there was a significant change in the particles size, from Zr-BTC to Ni/Zr-BTC, in which the size of the particles became smaller due to the mechanical process during Ni impregnation. Zr-BTC had an average particle size distribution of 6.447 ± 4.301 µm, whereas Ni/Zr-BTC was 5.516 ± 2.871 µm. The TEM image of the Zr-BTC displays a large distribution of particles with an average particle size of 39.9 nm (Figure 4(c) and Figure 4(e)). The presence of nickel and its distribution at Zr-BTC are observed as small black spots in the TEM image (Figure 4(d)) with an average Ni particle size of 10.8 nm (Figure 4(f)). The large spot might be resulted from the nickel agglomeration during the loading process. EDX analysis further confirmed the Ni loading, as shown in Table 1. Based on the EDX analysis, 2.25 wt.% Ni was successfully loaded into the Zr-BTC, which was slightly under estimated from the theoretical calculation (2.5 wt.%). This lower percentage might be resulted from the uneven distribution of Ni metal within Zr-BTC. Alternatively, Ni leaching during stirring, drying, and washing or reduction process after drying, might be possible as well.

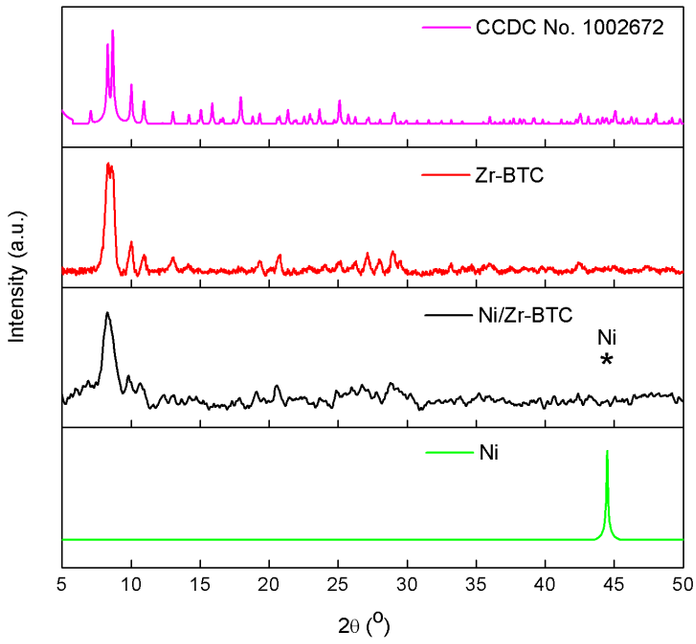

FIGURE 3. Diffractogram of CCDC standard No. 1002672, Zr-BTC, Ni/Zr-BTC and ICSD standard No. 64989

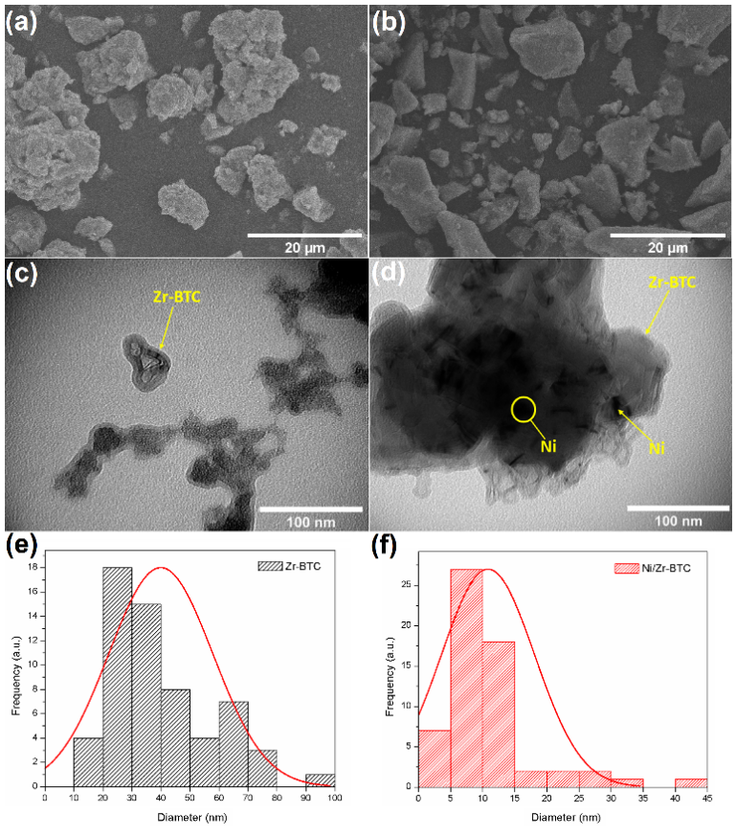

FIGURE 4. SEM images: (a) Zr-BTC synthesized, (b) Ni/Zr-BTC with 2,000× magnification and TEM images of c) Zr-BTC, d) Ni/Zr-BTC with 100,000× magnification, particle size distributions of e) Zr-BTC and f) Ni/Zr-BTC

TABLE 1. Element composition of Zr-BTC and Ni/Zr-BTC

Materials	Element composition (% weight)			
	O	C	Zr	Ni
Zr-BTC	45.91	41.84	12.25	-
Ni/Zr-BTC	37.14	20.89	39.70	2.25

The BET surface area, total pore volume, and pore size of the Zr-BTC and Ni/Zr-BTC materials are summarized in Table 2. The BET surface area of Ni/Zr-BTC (523 m^2/g) decreased relative to the pristine Zr-BTC (807 m^2/g). The pore size of both materials showed a similar trend, in which the pore volume of Zr-BTC was higher (0.27 cm^3/g) than that of Ni-loaded Zr-BTC (0.11 cm^3/g). This indicates that the surface area and pore volume of Zr-BTC decreased to 51.45% and 59.14%, respectively, after the loading of Ni. This phenomenon presumably occurred because Ni partially filled the pores of the Zr-BTC framework (Zhao et al. 2012). The empirical Ni metal diameter was 124 pm, while the Zr-BTC pore size was in the range of 17-19 Å (1700-1900 pm). Hence, some Ni metals could enter and occupy the Zr-BTC pores. This is consistent with a previous report, where the Ni loading into the MOF-5 structure remarkably decreased the surface area from 821.6 m^2/g (for MOF-5) to 619.9 m^2/g (for Ni@MOF-5), and the micropore volume decreased from 0.28 cm^3/g to 0.22 cm^3/g (Zhao et al. 2012).

TABLE 2. BET surface area analysis and pore volume on Zr-BTC and Ni/Zr-BTC

Materials	BET surface Area (m^2/g)	Pore volume (cm^3/g)	Pore size (Å)
Zr-BTC	807	0.27	18.9
Ni/Zr-BTC	523	0.11	19.7

The N_2 sorption isotherm curves of the synthesized Zr-BTC and Ni/Zr-BTC are shown in Figure 5(a). Zr-BTC adsorbed nitrogen higher than Ni/Zr-BTC. The adsorption-desorption isotherm curve also explains the absorption mechanism of Zr-BTC material following type IV adsorption isotherm, which indicates the capillary condensation within the mesopores (Ardila-Suárez et al. 2019). The pore volume was mostly filled at a relative pressure of less than 0.1, which indicates a strong microporous character (Ren et al. 2014). However, we observed that the adsorption-desorption lines on the Zr-BTC and Ni/Zr-BTC did not resemble to each other (Figure 5). The desorption curve was higher than the adsorption curve. These phenomena occur due to the presence of hysteresis loop in Zr-BTC and Ni/Zr-BTC (Ardila-Suárez et al. 2019). In the type IV isotherm, N_2 molecules will experience less desorption than their adsorption, leading to several N_2 molecules remaining in the pores due to the non-uniformity pore size of the material. An analysis of pore size distribution is presented in Figure 5(b). The pore size distribution graph confirmed that Zr-BTC and Ni/Zr-BTC had pores up to 18-19 Å. Zr-BTC had a pore diameter of 18.9 Å but after the Ni impregnation, the pore diameter became larger (19.7 Å, Table 2). This should be related to the metal aggregates formed on the surface of Zr-BTC (Simsek et al. 2013) synthesis and characterization of novel adsorbents based on natural zeolite (clinoptilolite).

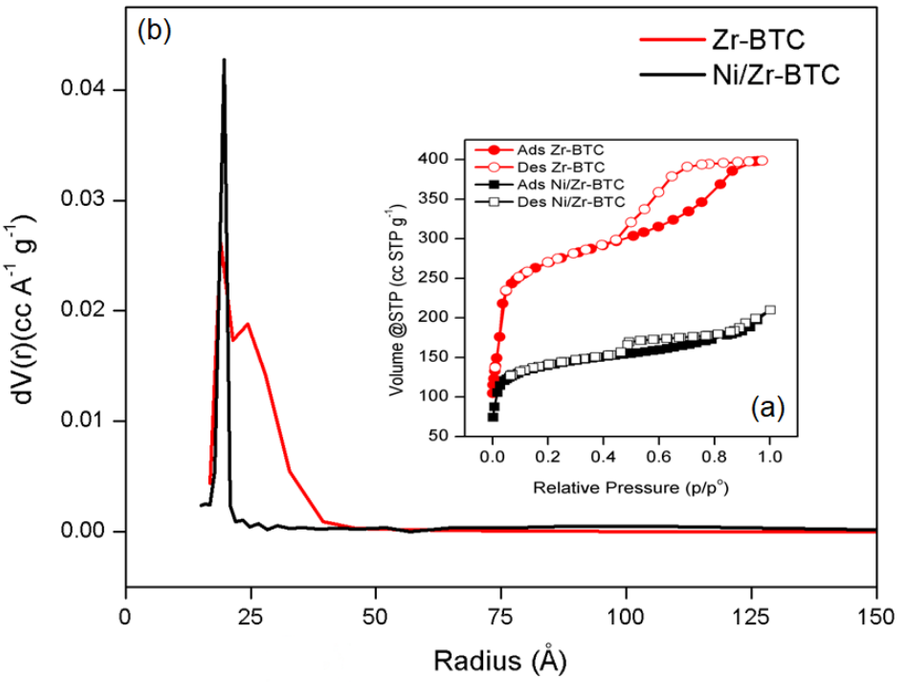

FIGURE 5. N_2 adsorption-desorption isotherm curves (a) and pore distribution graph of Zr-BTC and Ni/Zr-BTC (b)

Thermogravimetric analysis using TG/DTA was performed to verify the effect of Ni loading on the thermal stability of the Zr-BTC. Zr-BTC was stable up to 600 °C, as shown in the ESI (Figure S3). There were two decreasing curves on the thermogram, including the first mass loss that reached 29.2% at 35-149 °C, showing solvent (water and DMF) loss from the Zr-BTC framework. Based on the calculation, 32 H_2O molecules and three DMF molecules were released. Furthermore, the second mass loss reached 29.6% at 149-589 °C, indicating that the acetate group from the modulator began to disappear. However, in previous studies, the loss of the modulator was up to 210 °C (Bueken et al. 2014), followed by ligand decomposition (BTC^{3-}) from the Zr-BTC framework. In that study, the linker decomposition occurred between 210 °C and 350 °C (Bueken et al. 2014).

Ni impregnation on the Zr-BTC did not affect thermal stability, but it could reduce the first mass decrease to 18.9%. This might be due to the loss of residual solvent trapped in the pores during the impregnation and reduction processes. In particular, Ni/Zr-BTC thermogram exhibited a third mass decrease of 15.4% since there might be residues of a mixture of metal oxides originating from the initial Zr-BTC synthesis process and Ni metal impregnation process (Le et al. 2016; Nagai et al. 2015).

CATALYTIC TEST ON CITRONELLAL HYDROGENATION REACTION

Qualitative analysis of the product was performed using FTIR by comparing the spectra of the hydrogenation product with the spectra of the citronellal compound as the initial substrate. FTIR characterization can identify the specific functional groups of the product. According to the FTIR spectra in Figure 6, the hydrogenation product with a Ni/Zr-BTC catalyst produced a new widening absorption band at 3250-3600 cm^{-1} attributed to the –OH stretching vibration. The vibration bands at 1397-1456 cm^{-1} correspond to the $–CH_2–$ and –CH vibrations. Furthermore, the absorption of the C=O group was also observed in the range of 1655-1740 cm^{-1}, demonstrating the characteristics of citronellal as the starting material (Müller et al. 2016). The new absorption band at 1023 cm^{-1} may be from the C–O stretching vibration (primary alcohol), while the absorption band at 1166 cm^{-1} originated from the C–O stretching vibration (secondary alcohol) (Silverstein et al. 2005).

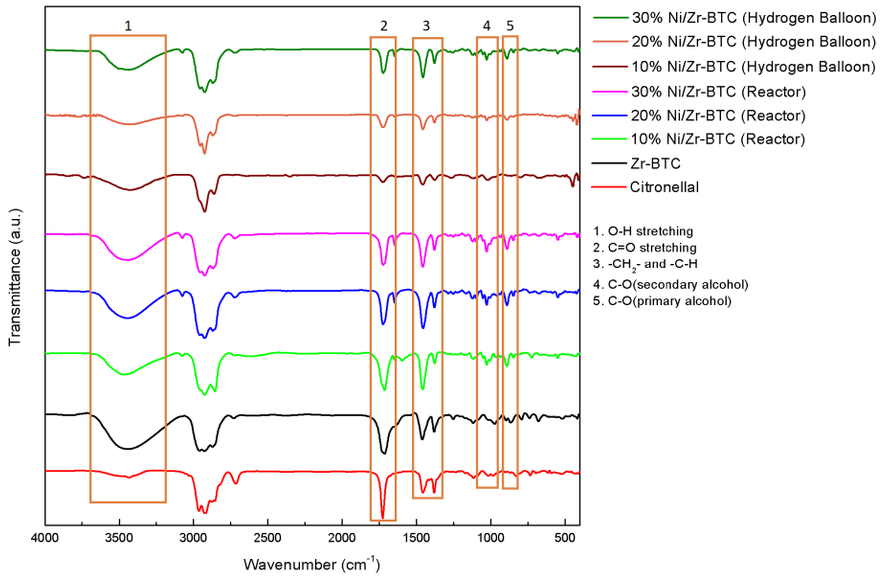

FIGURE 6. FTIR spectra of citronellal hydrogenation product after the reaction catalyzed by Zr-BTC and Ni/Zr-BTC catalysts

The presence of Ni in the Zr-BTC structure as catalyst can further convert citronellal in hydrogenation reaction. As shown in Figure 6 and Table 3, the intensity of the C=O absorption peak of citronellal can be reduced up to 99%. It also shows that the higher Ni loading in Zr-BTC, the sharper the C–O (primary alcohol) absorption at 1023 cm^{-1} was formed, suggesting the increase of primary alcohol compounds as citronellal hydrogenation products (O'Brien & Wicht 2008; Yu et al. 2000). A secondary alcohol product was also formed, as demonstrated by the presence of a C–O (secondary alcohol) absorption band at 1166 cm^{-1} (Silverstein et al. 2005). The hydrogenation efficiency, indicated by reducing the intensity of the transmittance ratio (C=O/C–O), reflecting the decrease of this functional group from citronellal as the starting material (Table 3). The products of the reaction performed in hydrogen balloon showed a significant decrease in oxygen content than those of the batch reactor system. The decrease in oxygen content was also observed from the dramatic change in the C=O absorption peak around 1655-1740 cm^{-1} (Hadjiivanov et al. 2021).

A quantitative analysis was carried out to determine the product distribution of the hydrogenation reaction (Figure 8, Table 4). Using the balloon system with 1 bar of hydrogen, we observed an enhancement in catalyst performance by increasing Ni loading in the hydrogenation reactions. These results indicate that the higher the nickel loading, the higher the catalytic activity. Similar results were observed for the hydrogenation

TABLE 3. The transmittance ratio of C=O/C–O from the hydrogenation product catalysed by Zr-BTC and Ni/Zr-BTC compared to the starting material analysed by FTIR spectroscopy

Catalysts	C=O (1726 cm^{-1})	C–O (1023 cm^{-1})	%T Ratio C=O/C–O
No Catalyst⁑	90.2	31.3	2.8
Zr-BTC*	49.8	45.3	1.1
10% Ni/Zr-BTC*	14.8	16.0	0.9
20% Ni/Zr-BTC*	0.6	1.6	0.3
30% Ni/Zr-BTC*	40.4	34.5	1.1
10% Ni/Zr-BTC⁑	54.4	38.5	1.4
20% Ni/Zr-BTC⁑	57.4	47.0	1.2
30% Ni/Zr-BTC⁑	35.9	32.3	1.1

Note: *(balloon), ⁑(reactor)

reaction using a batch reactor (10 bar). These results also show that the higher the Ni content loaded, the higher the catalytic performance. In addition, the high hydrogen pressure used in the reaction also increased the catalytic activity (1 bar in the balloon system vs. 10 bar in the reactor system). Based on the GC-MS analyses, the product of the hydrogenation reaction was partly citronellol, although other alcohol compounds, such as isopulegol, were quite dominant due to the isomerization reaction that produces an unsaturated cyclic product.

The cyclization product of citronellal to unsaturated cyclic alcohols (isopulegol) has a higher conversion rate (balloon and reactor systems) than without a catalyst (Table 4). Overall, the yield on cyclization to isopulegol is enhanced with an increase in the amount of nickel used in as catalyst (30% Ni > 20% Ni > 10% Ni). In this case, we propose that Ni interacts with hydrogen via a spillover mechanism to form an intermediate species, Ni–H. Thus, it can open the double bonds in the aliphatic chain and reduce the double bonds in the aldehyde group (Bettahar 2020). Subsequently, the cyclization mechanism takes place through the adjacent Brønsted acid site leading to the formation of isopulegol (Figure 7) (Yongzhong et al. 2005). According to Chuah et al. (2001), the citronellal cyclization comprises the protonation of the carbonyl group on citronellal by the acid site, followed by the intramolecular rearrangement to form a more stable carbocation and finally deprotonation to yield isopulegol (Mäki-Arvela et al. 2004).

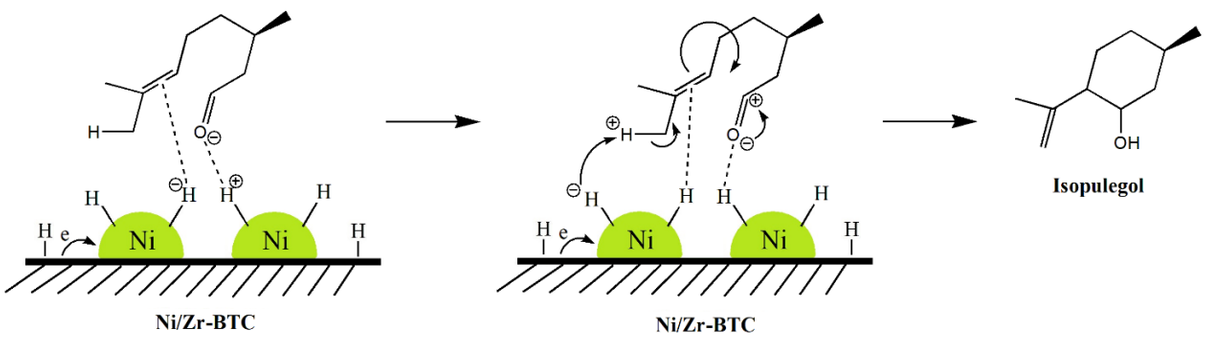

FIGURE 7. Proposed mechanism for cyclisation of citronellal to form isopulegol over Ni/Zr-BTC catalyst

The product of cyclization to isopulegol was still higher than the product of citronellal hydrogenation to citronellol in both reaction systems (hydrogen balloon and reactor). Nie et al. (2007) reported that increasing nickel loading negatively affected the cyclization of citronellal but had a positive effect on the hydrogenation reaction. When the H_2 pressure was 1 bar (balloon), the product of isopulegol (cyclic) was lower than reactor system. In contrast, at 10 bar H_2, the rate of hydrogenation of citronellal to citronellol (unsaturated alcohols) in the reactor was lower than in the balloon system (Table 4). Thus, the selectivity of the hydrogenation citronellal to citronellol was preferred in the hydrogen balloon system (Figure 9). This is another indication that the cyclization of citronellal could have occurred on the external surfaces of the Zr-BTC or on nickel crystallites, where the directing effect due to the micropores was absent (Figure 5) (Nie et al. 2007).

The distribution product of citronellal hydrogenation is displayed in Figure 8. Hydrogenation of citronellal produced several types of products, including unsaturated alcohols produced from the hydrogenation of only the C=O group and saturated alcohol products produced from the hydrogenation of the C=O and C=C groups. In other words, the C=C group is hydrogenated only after the C=O group has been hydrogenated. The saturated alcohol exhibited a high yield, reaching 4.2-7.7%, whereas the unsaturated alcohol had a lower yield (1.8-6.3%). These unsaturated alcohol products can either desorb from the catalytic surface or further hydrogenate to the saturated alcohols if allowed to continue to react (Ide et al. 2012). As a result, significant amounts of saturated alcohols can form during the reaction, which is in line with the experimental results (Table 4 & Figure 10). The selectivity towards citronellol of Ni/Zr-BTC catalyst is enhanced by the increase of Ni concentration presence in the reaction, as shown in Figure 9. The selectivity of 10, 20, and 30% Ni/Zr-BTC catalysts using a hydrogen balloon are 2.1, 9.5 and 14.1%, respectively. On the other hand, using a batch reactor with 10, 20, and 30% Ni/Zr-

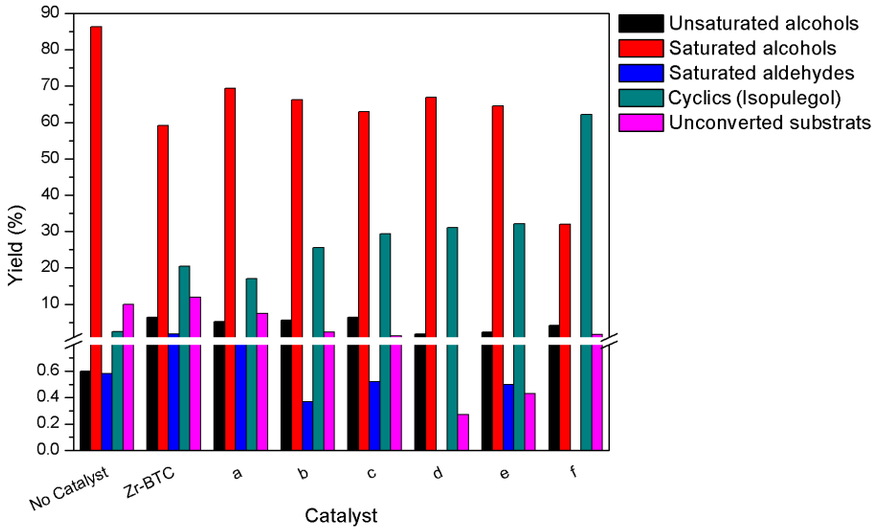

FIGURE 8. Distribution of citronellal hydrogenation products: (a) 10% Ni/Zr-BTC (balloon); (b) 20% Ni/Zr-BTC (balloon); (c) 30% Ni/Zr-BTC (balloon); (d) 10% Ni/Zr-BTC (reactor); (e) 20% Ni/Zr-BTC (reactor); (f) 30% Ni/Zr-BTC (reactor)

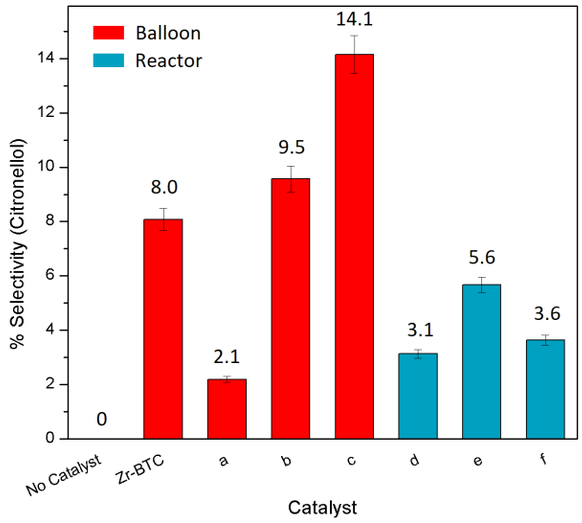

FIGURE 9. Catalytic selectivity of Ni/Zr-BTC on citronellol formation: (a) 10% Ni/Zr-BTC (balloon); (b) 20% Ni/Zr-BTC (balloon); (c) 30% Ni/Zr-BTC (balloon); (d) 10% Ni/Zr-BTC (reactor); (e) 20% Ni/Zr-BTC (reactor); (f) 30% Ni/Zr-BTC (reactor)

BTC catalysts resulted in the product selectivity of 3.1, 5.6, and 3.6%, respectively. The selectivity to citronellol was higher with a hydrogen balloon (30% Ni) than with a batch reactor. The adsorbed Ni were thought to stimulate the C=O double bonds, speeding up the process and increasing selectivity for unsaturated alcohols.

According to Claus (1998), the thermodynamically stable unsaturated alcohols are more difficult to obtain compared to saturated alcohols because the C=C bond energy is lower than the C=O bond energy. As a result, the C=C bond is more easily hydrogenated (Ide et al. 2012). Thus, the formation of saturated alcohol is favoured,

although other reactions may occur apart from the formation of citronellol. The C=O bond in the citronellal could be polarized, and the electron cloud density in the C=O bond could be reduced due to the Lewis acid site from nickel. The Zr-BTC frameworks could facilitate a more efficient substrate adsorption and easier interaction of nickel and hydrogen species. The hydrogen molecules are splitted to hydrogen atom via spillover mechanism and will interact with nickel to become Ni–H reactive species and take place in the catalytic reaction (Figure 10). In this hydrogenation reaction, the higher the Ni metal presence, the higher the hydrogen available in the reaction. Therefore, the activity of Ni/Zr-BTC catalyst increases due to the high Ni metal presence. Nie et al. (2007) reported that Ni/Al-MCM-41 exhibited high activity in the hydrogenation of citronellal into menthol with a 90% selectivity. Ni has shown to increase the activity of the catalyst in the hydrogenation of citronellal (Sudiyarmanto et al. 2020).

TABLE 4. Distribution of hydrogenation products of citronellal

Catalyst	Yield (%)				
	Unsaturated alcohols	Saturated alcohols	Saturated aldehydes	Cyclics (Isopulegol)	Unconverted substrates
No catalyst‡	0.6	86.3	0.58	2.42	10.0
Zr-BTC*	6.4	59.2	1.8	20.5	11.9
10% Ni/Zr-BTC*	5.2	69.4	0.8	16.9	7.4
20% Ni/Zr-BTC*	5.5	66.2	0.3	25.5	2.3
30% Ni/Zr-BTC*	6.3	62.9	0.5	29.4	1.2
10% Ni/Zr-BTC‡	1.8	66.8	0	31.0	0.2
20% Ni/Zr-BTC‡	2.3	64.5	0.5	32.1	0.4
30% Ni/Zr-BTC‡	4.1	32.0	0	62.1	1.6

Note: *(balloon), ‡(reactor)

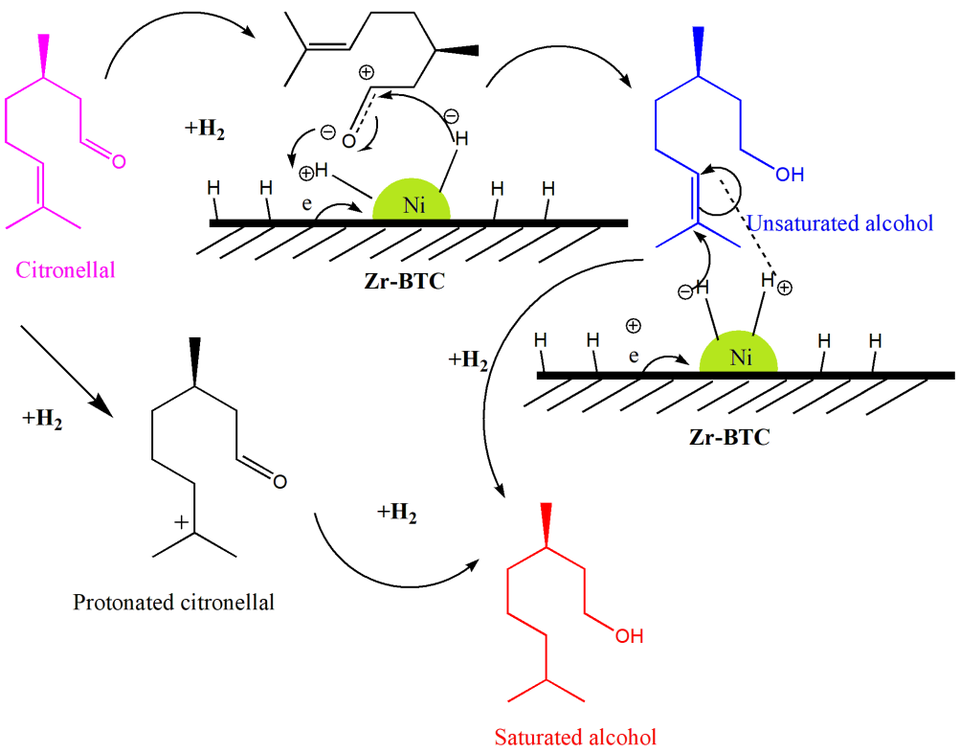

FIGURE 10. Proposed mechanism of catalytic reaction using Ni/Zr-BTC in hydrogenation reaction of citronellal to form saturated and unsaturated alcohols

In this study, citronellal hydrogenation reactions were carried out using two different systems; a batch reactor and a hydrogen balloon. Both methods offered different catalytic performances. The activity and selectivity of the citronellal hydrogenation reaction were affected by the type of solvent used in the reaction. In the experiment, 2-propanol was used as the solvent since it is more selective in assisting the reduction of the C=O bond than the C=C bond. The hydroxyl group in the 2-propanol could form the hydrogen bond with the O atom in the carbonyl group of citronellal compound. Consequently, the O atom of the carbonyl group of the citronellal became polarized, and the electron cloud density around the C=O bond is decreased, which enhanced the hydrogenation reaction (Mertens et al. 2006; Qu et al. 2015). In this case, catalytic transfer hydrogenation was also occurred, as illustrated in the proposed reaction mechanism in Figure 11.

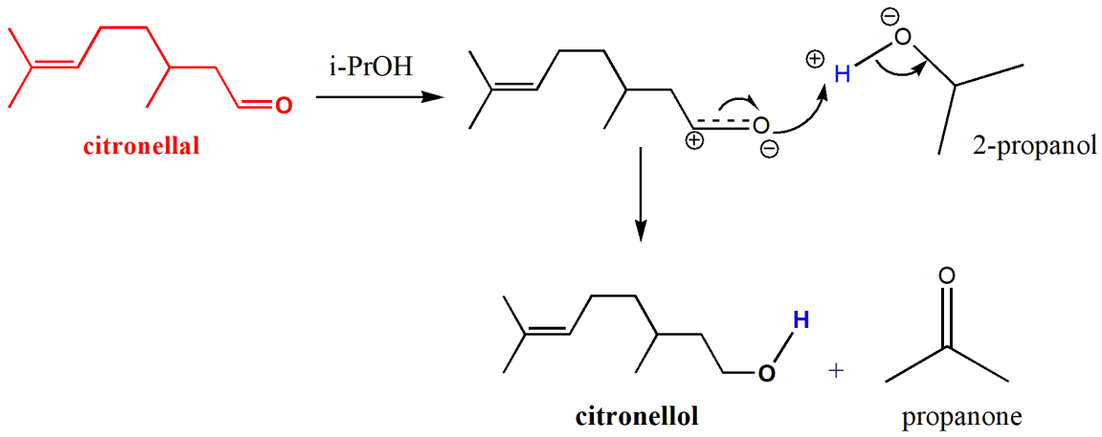

FIGURE 11. The 2-propanol solvent's effect on citronellol formation

CONCLUSIONS

Zr-BTC has been successfully impregnated with Ni and employed as a catalyst in the hydrogenation of citronellal. In this study, Ni loading did not change the framework's chemical structure, purity, or thermal stability of Zr-BTC. However, it affected the morphology and reduced the crystallinity, surface area, and pore volume of Zr-BTC. Ni loading enhanced the catalytic performance of Zr-BTC in the hydrogenation of citronellal, and led to the formation of unsaturated alcohol products. The citronellal hydrogenation reaction, which was carried out using a batch reactor and a hydrogen balloon, yielded different performances. The catalyst test using a batch reactor tended to increase the catalytic activity, whereas the catalytic test using a hydrogen balloon was more selective to produce unsaturated alcohol with citronellol products up to 14.1% using 30% Ni/Zr-BTC. The hydrogenation reaction under batch reactor condition was more active for the cyclization reaction with 62.1% of isopulegol product using 30% Ni/Zr-BTC.

ACKNOWLEDGEMENTS

We would like to acknowledge The Ministry of High Education, Culture, Research, and Technology of Republic Indonesia (RISTEK DIKTI) through the scheme World Class Research (WCR) 2021 Project number 2104/UN27.22/PT.01.03/2021.

REFERENCES

Ardila-Suárez, C., Díaz-Lasprilla, A.M., Díaz-Vaca, L.A., Balbuena, P.B., Baldovino-Medrano, V.G. & Ramírez-Caballero, G.E. 2019. Synthesis, characterization, and post-synthetic modification of a micro/mesoporous zirconium-tricarboxylate metal-organic framework: Towards the addition of acid active sites. *CrystEngComm* 21(19): 3014-3030.

Bai, Y., Dou, Y., Xie, L.H., Rutledge, W., Li, J.R. & Zhou, H.C. 2016. Zr-based metal-organic frameworks: Design, synthesis, structure, and applications. *Chemical Society Reviews* 45(8): 2327-2367.

Bettahar, M.M. 2020. The hydrogen spillover effect. A misunderstanding story. *Catalysis Reviews - Science and Engineering* 64(1): 87-125.

Bueken, B., Reinsch, H., Reimer, N., Stassen, I., Vermoortele, F., Ameloot, R., Stock, N., Kirschhock, C.E.A. & De Vos, D. 2014. A zirconium squarate metal-organic framework with modulator-dependent molecular sieving properties. *Chemical Communications* 50(70): 10055-10058.

Cavka, J.H., Jakobsen, S., Olsbye, U., Guillou, N., Lamberti, C., Bordiga, S. & Lillerud, K.P. 2008. A new zirconium inorganic building brick forming metal organic frameworks with exceptional stability. *Journal of the American Chemical Society* 130(42): 13850-13851.

Chuah, G.K., Liu, S.H., Jaenicke, S. & Harrison, L.J. 2001. Cyclisation of citronellal to isopulegol catalysed by hydrous zirconia and other solid acids. *Journal of Catalysis* 200(2): 352-359.

Cirujano, F.G., Corma, A. & Xamena, F.X.L.I. 2015. Conversion of Levulinic acid into chemicals: Synthesis of biomass derived levulinate esters over Zr-containing MOFs. *Chemical Engineering Science* 124: 52-60.

Cirujano, F.G., Corma, A. & Xamena, F.X.L.I. 2012. MOFs as multifunctional catalysts: One-pot synthesis of menthol from citronellal over a bifunctional MIL-101 catalyst. *Dalton Transactions* 41(14): 4249-4254.

Claus, P. 1998. Selective hydrogenation of α,β-unsaturated aldehydes and other C=O and C=C bonds containing compounds. *Topics in Catalysis* 5: 51-62.

Feng, D., Gu, Z.Y., Li, J.R., Jiang, H.L., Wei, Z. & Zhou, H.C. 2012. Zirconium-metalloporphyrin PCN-222: Mesoporous metal-organic frameworks with ultrahigh stability as biomimetic catalysts. *Angewandte Chemie - International Edition* 51(41): 10307-10310.

Furukawa, H., Gándara, F., Zhang, Y.B., Jiang, J., Queen, W.L., Hudson, M.R. & Yaghi, O.M. 2014. Water adsorption in porous metal-organic frameworks and related materials. *Journal of the American Chemical Society* 136(11): 4369-4381.

Genna, D.T., Pfund, L.Y., Samblanet, D.C., Wong-Foy, A.G., Matzger, A.J. & Sanford, M.S. 2016. Rhodium hydrogenation catalysts supported in metal organic frameworks: Influence of the framework on catalytic activity and selectivity. *ACS Catalysis* 6(6): 3569-3574.

Guenther, E. 1982. *The Essential Oils: Individual Essential Oils of the Plant Families Gramineae, Lauraceae, Burseraceae, Myrtaceae, Umbelliferae and Geraniaceae.* Krieger, R.E. Publishing Company. p. 507.

Hadjiivanov, K.I., Panayotov, D.A., Mihaylov, M.Y., Ivanova, E.Z., Chakarova, K.K., Andonova, S.M. & Drenchev, N.L. 2021. Power of infrared and raman spectroscopies to characterize metal-organic frameworks and investigate their interaction with guest molecules. *Chemical Reviews* 121: 1286-1424.

Hanif, Q.A., Nugraha, R.E. & Lestari, W.W. 2018. Kajian metal-organic frameworks (MOFs) sebagai material baru pengantar obat. *ALCHEMY Jurnal Penelitian Kimia* 14(1): 16.

Horcajada, P., Surblé, S., Serre, C., Hong, D.Y., Seo, Y.K., Chang, J.S., Grenèche, J.M., Margiolaki, I. & Férey, G. 2007. Synthesis and catalytic properties of MIL-100(Fe), an iron(III) carboxylate with large pores. *Chemical Communications* 100(27): 2820-2822.

Hwang, Y.K., San Chang, J., Hong, D.Y., Hwang, D.W., Lee, U.H., Cho, K.H., Valekar, A.H. & Lee, S.K. 2017. Zirconium-based metal-organic frameworks as catalyst for transfer hydrogenation. https://patents.google.com/patent/US10195592B2/en. Accessed on 9 November 2017.

Ide, M.S., Hao, B., Neurock, M. & Davis, R.J. 2012. Mechanistic insights on the hydrogenation of α,β-unsaturated ketones and aldehydes to unsaturated alcohols over metal catalysts. *ACS Catalysis* 2(4): 671-683.

Kandiah, M., Nilsen, M.H., Usseglio, S., Jakobsen, S., Olsbye, U., Tilset, M., Larabi, C., Quadrelli, E.A., Bonino, F. & Lillerud, K.P. 2010. Synthesis and stability of tagged UiO-66 Zr-MOFs. *Chemistry of Materials* 22(24): 6632-6640.

Kim, M. & Cohen, S.M. 2012. Discovery, development, and functionalization of Zr(Iv)-based metal-organic frameworks. *CrystEngComm* 14(120): 4096-4104.

Larasati, I., Winarni, D., Putri, F.R., Hanif, Q.A. & Lestari, W.W. 2017. Synthesis of metal-organic frameworks based on Zr^{4+} and benzene 1,3,5-tricarboxylate linker as heterogeneous catalyst in the esterification reaction of palmitic acid. *IOP Conference Series: Materials Science and Engineering* 214: 012006.

Le, T.D., Nguyen, K.D., Nguyen, V.T., Truong, T. & Phan, N.T.S. 2016. 1,5-benzodiazepine synthesis via cyclocondensation of 1,2-diamines with ketones using iron-based metal-organic framework MOF-235 as an efficient heterogeneous catalyst. *Journal of Catalysis* 333: 94-101.

Lestari, W.W., Prajanira, L.B., Putra, R., Purnawan, C., Prihadiyono, F.I. & Arrozi, U.S.F. 2021. Green-synthesized MIL-100(Fe) modified with palladium as a selective catalyst in the hydrogenation of citronellal to citronellol. *Materials Research Express* 8(April 1): 045504.

Li, Y.Z., Wang, H.H., Yang, H.Y., Hou, L., Wang, Y.Y. & Zhu, Z. 2018. An uncommon carboxyl-decorated metal–organic framework with selective gas adsorption and catalytic conversion of CO_2. *Chemistry - A European Journal* 24(4): 865-871.

Liang, W., Chevreau, H., Ragon, F., Southon, P.D., Peterson, V.K. & D'Alessandro, D.M. 2014. Tuning pore size in a zirconium-tricarboxylate metal-organic framework. *Crystal Engineering Community* 16: 6530-6533.

Mäki-Arvela, P., Kumar, N., Nieminen, V., Sjöholm, R., Salmi, T. & Murzin, D.Y. 2004. Cyclization of citronellal over zeolites and mesoporous materials for production of isopulegol. *Journal of Catalysis* 225(1): 155-169.

Mertens, P., Verpoort, F., Parvulescu, A.N. & De Vos, D. 2006. Pt/H-beta zeolites as productive bifunctional catalysts for the one-step citronellal-to-menthol conversion. *Journal of Catalysis* 243(1): 7-13.

Milone, C., Gangemi, C., Ingoglia, R., Neri, G. & Galvagno, S. 1999. Role of the support in the hydrogenation of citronellal on ruthenium catalysts. *Applied Catalysis A: General* 184: 89-94.

Morris, W., Volosskiy, B., Demir, S., Gándara, F., McGrier, P.L., Furukawa, H., Cascio, D., Stoddart, J.F. & Yaghi, O.M. 2012. Synthesis, structure, and metalation of two new highly porous zirconium metal-organic frameworks. *Inorganic Chemistry* 51(12): 6443-6445.

Müller, P., Wolf, P. & Hermans, I. 2016. Insights into the complexity of heterogeneous liquid-phase catalysis: Case study on the cyclization of citronellal. *ACS Catalysis* 6(5): 2760-2769.

Nagai, D., Nishibori, M., Itoh, T., Kawabe, T., Sato, K. & Shin, W. 2015. Ppm level methane detection using micro-thermoelectric gas sensors with Pd/Al_2O_3 combustion catalyst films. *Sensors and Actuators B: Chemical* 206: 488-494.

Nie, Y., Niah, W., Jaenicke, S. & Chuah, G.K. 2007. A tandem cyclization and hydrogenation of (±)-citronellal to menthol over bifunctional Ni/Zr-beta and mixed Zr-beta and Ni/MCM-41. *Journal of Catalysis* 248: 1-10.

O'Brien, K.E. & Wicht, D.K. 2008. A greener organic chemistry experiment: Reduction of citronellal to citronellol using poly(methylhydro)siloxane. *Green Chemistry Letters and Reviews* 1(3): 149-154.

Park, Y.K., Choi, S.B., Nam, H.J., Jung, D.Y., Ahn, H.C., Choi, K., Furukawa, H. & Kim, J. 2010. Catalytic nickel nanoparticles embedded in a mesoporous metal-organic framework. *Chemical Communications* 46(18): 3086-3088.

Plessers, E., Fu, G., Tan, C.Y.X., De Vos, D.E. & Roeffaers, M.B.J. 2016. Zr-based MOF-808 as meerwein–ponndorf–verley reduction catalyst for challenging carbonyl compounds. *Catalysts* 6(7): 104.

Putra, R., Lestari, W.W., Wibowo, F.R. & Susanto, B.H. 2018. Fe/Indonesian natural zeolite as hydrodeoxygenation catalyst in green diesel production from palm oil. *Bulletin of Chemical Reaction Engineering & Catalysis* 13(2): 245-255.

Qneibi, M., Jaradat, N. & Emwas, N. 2019. Effect of geraniol and citronellol essential oils on the biophysical gating properties of AMPA receptors. *Applied Sciences (Switzerland)* 9(21): 4693.

Qu, P.F., Chen, J.G., Song, Y.H., Liu, Z.T., Liu, Z.W., Li, Y., Lu, J. & Jiang, J. 2015. Effect of Fe(III) on hydrogenation of citral over Pt supported multiwalled carbon nanotube. *Catalysis Communications* 68(3): 105-109.

Reinsch, H., Bueken, B., Vermoortele, F., Stassen, I., Lieb, A., Lillerud, K.P. & De Vos, D. 2015. Green synthesis of zirconium-MOFs. *CrystEngComm* 17(22): 4070-4074.

Ren, J., Segakweng, T., Langmi, H.W., Musyoka, N.M., North, B.C., Mathe, M. & Bessarabov, D. 2014. Microwave-assisted modulated synthesis of zirconium-based metal-organic framework (Zr-MOF) for hydrogen storage applications. *International Journal of Materials Research* 105(5): 516-519.

Silverstein, R.M., Webster, F.X. & Kiemle, D.J. 2005. *Spectrometric Identification of Organic Compounds.* 7th ed. New York: John Wiley & Sons.

Simsek, E.B., Özdemir, E. & Beker, U. 2013. Zeolite supported mono- and bimetallic oxides: Promising adsorbents for removal of As(V) in aqueous solutions. *Chemical Engineering Journal* 220: 402-411.

Stassen, I., Styles, M., Van Assche, T., Campagnol, N., Fransaer, J., Denayer, J., Tan, J.C., Falcaro, P., De Vos, D. & Ameloot, R. 2015. Electrochemical film deposition of the zirconium metal-organic framework UiO-66 and application in a miniaturized sorbent trap. *Chemistry of Materials* 27(5): 1801-1807.

Sudiyarmanto, S., Adilina, I.B., Aditya, R.R., Sukandar, D. & Tursiloadi, S. 2020. Catalytic conversion of citronellal to citronellol over skeletal Ni catalyst. *Journal of Physics: Conference Series* 1442(1): 012047.

Užarević, K., Wang, T.C., Moon, S.Y., Fidelli, A.M., Hupp, J.T., Farha, O.K. & Friščić, T. 2016. Mechanochemical and solvent-free assembly of zirconium-based metal-organic frameworks. *Chemical Communications* 52(10): 2133-2136.

Xu, J., Liu, J., Li, Z., Wang, X. & Wang, Z. 2019. Synthesis, structure and properties of Pd@MOF-808. *Journal of Materials Science* 54(19): 12911-12924.

Yongzhong, Z., Yuntong, N., Jaenicke, S. & Chuah, G.K. 2005. Cyclisation of citronellal over zirconium zeolite beta - A highly diastereoselective catalyst to (±)-isopulegol. *Journal of Catalysis* 229(2): 404-413.

Yu, W., Liu, H., Liu, M. & Liu, Z. 2000. Selective hydrogenation of citronellal to citronellol over polymer-stabilized noble metal colloids. *Reactive and Functional Polymers* 44(1): 21-29.

Yuan, Q., Zhang, D., Van Haandel, L., Ye, F., Xue, T., Hensen, E.J.M. & Guan, Y. 2015. Selective liquid phase hydrogenation of furfural to furfuryl alcohol by Ru/Zr-MOFs. *Journal of Molecular Catalysis A: Chemical* 406: 58-64.

Yuan, S., Feng, L., Wang, K., Pang, J., Bosch, M., Lollar, C., Sun, Y., Qin, J., Yang, X., Zhang, P., Wang, Q., Zou, L., Zhang, Y., Zhang, L., Fang, Y., Li, J. & Zhou, H-C. 2018. Stable metal–organic frameworks: Design, synthesis, and applications. *Advanced Materials* 30(37): 1704303.

Zhao, H., Song, H. & Chou, L. 2012. Nickel nanoparticles supported on MOF-5: Synthesis and catalytic hydrogenation properties. *Inorganic Chemistry Communications* 15: 261-265.

Zhao, Z.W., Zhou, X., Liu, Y.N., Shen, C.C., Yuan, C.Z., Jiang, Y.F., Zhao, S.J., Ma, L.B., Cheang, T.Y. & Xu, A.W. 2018. Ultrasmall Ni nanoparticles embedded in Zr-based MOFs provide high selectivity for CO_2 hydrogenation to methane at low temperatures. *Catalysis Science and Technology* 8(12): 3160-3165.

Zhen, W., Gao, F., Tian, B., Ding, P., Deng, Y., Li, Z., Gao, H. & Lu, G. 2017. Enhancing activity for carbon dioxide methanation by encapsulating (1 1 1) facet Ni particle in metal–organic frameworks at low temperature. *Journal of Catalysis* 348: 200-211.

Zong, M., Fan, C., Yang, X. & Wang, D. 2021. Promoting Ni-MOF with metallic Ni for highly-efficient *p*-nitrophenol hydrogenation. *Molecular Catalysis* 509(March): 111609.

*Corresponding author; email: witri@mipa.uns.ac.id

Refinement of Zr(IV)-BTC based MOF and 2.5% Ni/Zr-BTC using Le-Bail Method

a) Refinement of Material Zr(IV)-BTC based MOF

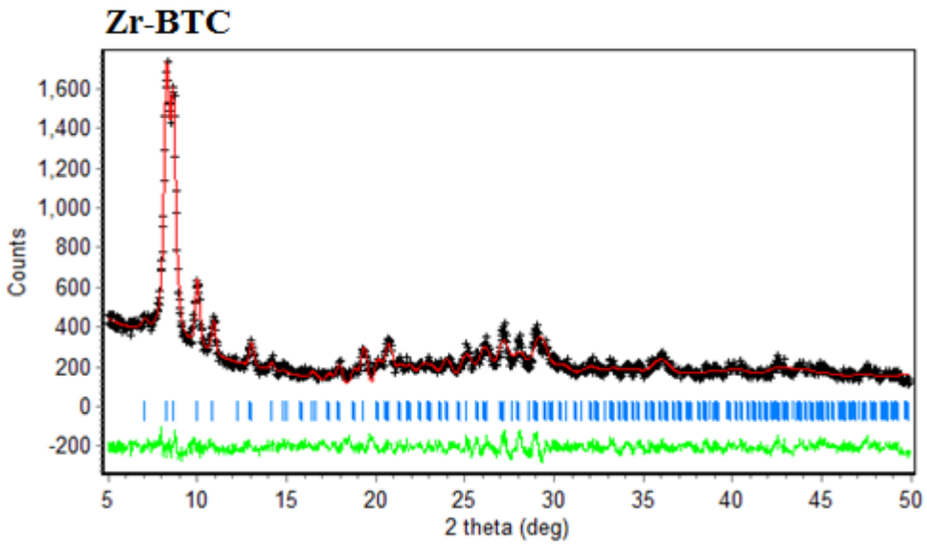

FIGURE S1. Refinement curve of Zr-BTC

b) Refinement of 2.5% Ni/Zr-BTC

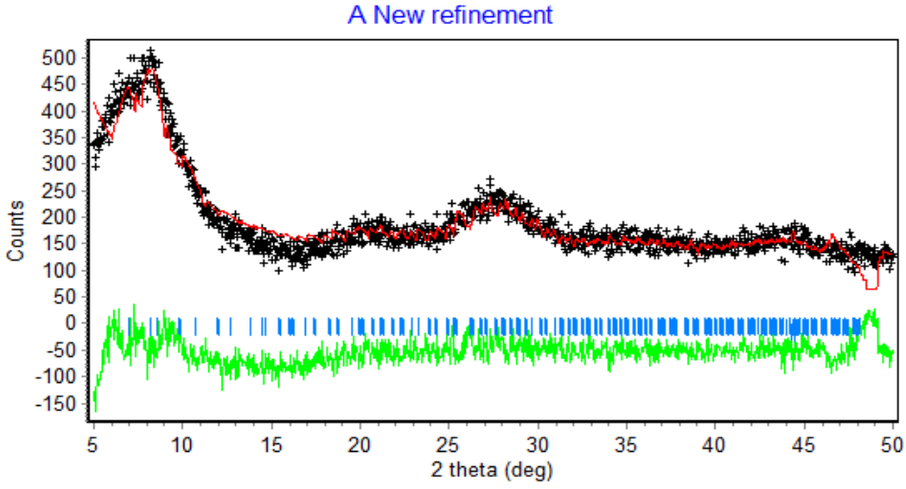

FIGURE S2. Refinement curve of Zr-BTC modified Ni

TABLE S1. Refinement Results of Zr-BTC and Ni/Zr-BTC

Refinement result	Zr-BTC	2.5% Ni/Zr-BTC
$\%R_p$	7.09	8.249
$\%R_{wp}$	4.79	8.648
GoF	0.231	0.4615

TABLE S2. Cell parameter from H_3BTC ligand and Zr-BTC (Furukawa et al. 2014)

Cell parameter	H_3BTC ligand	Zr-BTC
Crystal system	Monoclinic	Cubic
Space group	C2/c	Fd-3m
Length (Å)	a : 26.520 b : 16.420 c : 26.551	a : 35.0764 b : 35.0764 c : 35.0764
Angle (°)	α : 90 β : 91.53 γ : 90	α : 90 β : 90 γ : 90
Z	48	16

1. a. Thermogravimetry analysis of Zr-BTC and Ni/Zr-BTC

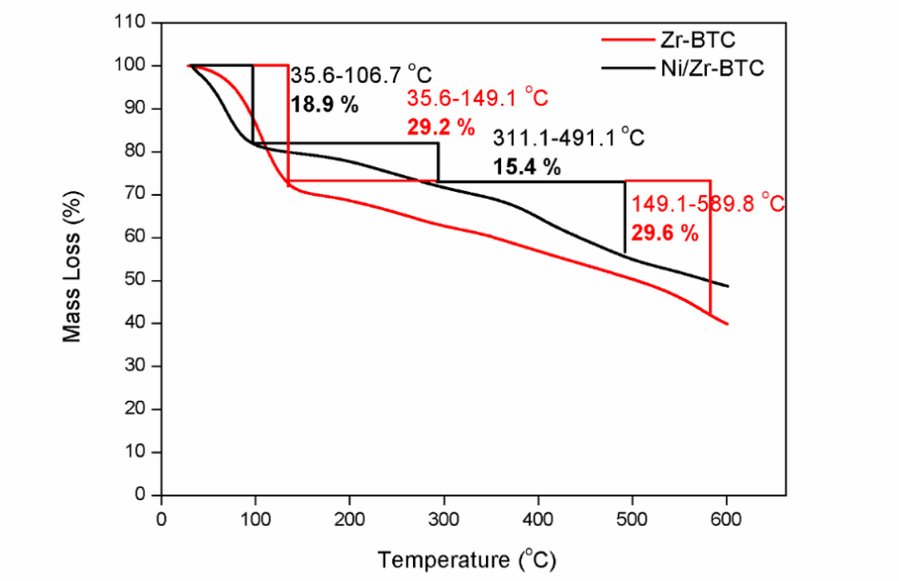

FIGURE S3. Thermogram of material Zr-BTC dan Ni/Zr-BTC

b. Mass loss calculation on material Zr-BTC

• *1st mass loss*

X = 149.0827 (Temperature)

Y = 70.758

Temperature decrease = 35.66153 °C - 149.0827 °C

% mass loss = 100% - 70.758%

= 29.242%

$$\text{Mw loss} = \text{Mw Zr-BTC} \left(\frac{\%\ \text{Mass loss}}{1-\%\ \text{Mass loss}}\right)$$

$$= 2023.6 \left(\frac{29.242\ \%}{1-29.242\ \%}\right)$$

$$= 2023.6 \left(\frac{0.29242}{1-0.29242}\right)$$

$$= 2023.6\ (0.4132677577)$$

$$= 836.2886345007\ \text{g/mol}$$

Mw of 32 molecules H_2O = 32 × 18 g/mol = 576 g/mol
(according to macular formula)
Mr of the remaining molecules = 836.2886345007 g/mol - 576 g/mol = 260.2886345007 g/mol
The loss of DMF molecules = 260.2886345007 g/mol / 73.09 g/mol = 3.5612072035 ~ 3 DMF molecules

- *The 2nd mass loss*

X = 589.8937 (Temperature)
Y = 41.08819
Temperature decrease = 149.0827 °C - 589.8937 °C
% Mass loss = 70.758% - 41.08819% = 29.66981

$$\%\text{Wt loss} = \text{Mw Zr-BTC} \left(\frac{\%\ \text{Mass loss}}{1-\%\ \text{Mass loss}}\right)$$

$$= 2023.6 \left(\frac{29.66981\ \%}{1-29.66981\ \%}\right)$$

$$= 2023.6 \left(\frac{0.2966981}{1-0.2966981}\right)$$

$$= 2023.6\ (0.4218644938)$$

$$= 853.6849895614\ \text{g/mol}$$

Mw of 6 CH_3COOH molecules = 6 × 60.052 g/mol
(according to molecular formula) = 360.312 g/mol
Mw of 2 ligand (H_3BTC) molecules = 2 × 210.14 g/mol
(according to molecular formula) = 420.28 g/mol

c. Mass loss calculation of water content in Zr-BTC structure

Formula: $[Zr_6O_4(OH)_4(CH_3COO)_6(BTC)_2].32H_2O$

Mw without H_2O = 1447.6 g/mol

Mw H_2O = 18 g/mol

% mass of H_2O loss = 29%

Σ n H_2O = ... ?

$$\%\ \text{mass loss} = \frac{\text{Mw of H2O loss}}{\text{Mw without H2O + Mw H2O loss}} \times 100\%$$

$$29\% = \frac{\text{Mr H2O loss}}{1447.6\ \text{g/mol + Mw H2O loss}} \times 100\%$$

$$0.29 = \frac{\text{Mw H2O loss}}{1447.6\ \text{g/mol + Mw H2O loss}}$$

Mw H_2O loss = 419.8 g/mol + 0.29 Mw H_2O loss
0.71 Mw H_2O loss = 419.8 g/mol
Mw H_2O loss = 591,27 g/mol
b. Σ n H_2O
Σ n H_2O = Mr H_2O loss/Mw H_2O
= 591.27 g/mol/18 g/mol
= 32 H_2O molecules